Med Biol Eng Comput (2009) 47:861–873
DOI 10.1007/s11517-009-0497-1

SPECIAL ISSUE - ORIGINAL ARTICLE

Ultrasonic characterization of ultrasound contrast agents

Nico de Jong · Marcia Emmer · Annemieke van Wamel · Michel Versluis

Received: 4 February 2009 / Accepted: 16 April 2009 / Published online: 26 May 2009

Abstract The main constituent of an ultrasound contrast agent (UCA) is gas-filled microbubbles. An average UCA contains billions per ml. These microbubbles are excellent ultrasound scatterers due to their high compressibility. In an ultrasound field they act as resonant systems, resulting in harmonic energy in the backscattered ultrasound signal, such as energy at the subharmonic, ultraharmonic and higher harmonic frequencies. This harmonic energy is exploited for contrast enhanced imaging to discriminate the contrast agent from surrounding tissue. The amount of harmonic energy that the contrast agent bubbles generate depends on the bubble characteristics in combination with the ultrasound field applied. This paper summarizes different strategies to characterize the UCAs. These strategies can be divided into acoustic and optical methods, which focus on the linear or nonlinear responses of the contrast agent bubbles. In addition, the characteristics of individual bubbles can be determined or the bubbles can be examined when they are part of a population. Recently, especially optical methods have proven their value to study individual bubbles. This paper concludes by showing some examples of optically observed typical behavior of contrast bubbles in ultrasound fields.

N. de Jong (✉) · M. Emmer · A. van Wamel
Biomedical Engineering (Thoraxcenter),
Erasmus University Medical Center,
Rotterdam, The Netherlands
e-mail: n.dejong@erasmusmc.nl

M. Versluis
Physics of Fluids, University of Twente,
Enschede, The Netherlands

1 Introduction

Ultrasound contrast agents (UCAs) have been commercially available since 1991. Echovist (Bayer Schering Pharma AG) was the first agent that was introduced on the market. It was mainly used to image ventricular septal defects and to investigate the female genital tract. The intravascular life-time of Echovist was too short for a transit through the pulmonary circulation. For cardiac blood flow and perfusion measurements, more stable UCAs came available such as Albunex in 1994 and Levovist in 1996. These first contrast agents have in common that they consist of fluids containing air-filled microbubbles. These microbubbles are stabilized to prevent a quick dissolution. Echovist and Levovist find their stability in the sugars containing air pockets and Albunex microbubbles are encapsulated by a shell composed of human albumin. UCAs that are currently marketed contain gases with a higher molecular weight than air and are stabilized by flexible coatings such as phospholipid surfactants. Commercial UCAs currently available are Optison (GE Healthcare, Chalfont St Giles, UK), Definity (Lantheus Medical Imaging, North Billerica, MA, USA), SonoVue (Bracco, Milan, Italy), and Sonazoid (GE Healthcare, Chalfont St Giles, UK). The adaptations to the gas content and coating have led to contrast agents with an improved lifespan and a wider use in the clinic.

The use of UCAs is largely determined by the physical properties of the coated microbubbles that the UCAs contain. In this chapter, we present a number of instruments to characterize UCAs. These instruments can be roughly divided into simulations and experiments. First, the influence of the gas content and coating on the physical properties of the coated microbubbles is discussed. In Sect. 3, equations that describe the vibrations of the contrast agent

microbubbles in an acoustic field are presented. These equations are the basis for theoretical characterization of the UCAs. In experiments, the responses of UCAs can be characterized acoustically as well as optically. We describe in Sect. 4 acoustical experiments that are performed on a population of microbubbles. These types of experiments are relatively easy to perform, but they do not show how individual microbubbles respond in an acoustic field. A fast framing camera offers great possibilities to study individual microbubbles. Section 5 presents methods to characterize individual microbubbles using such a fast framing camera system. Some interesting optical observations conclude this chapter.

2 Stability of coated microbubbles

UCAs contain bubbles with sizes between 1 and 10 μm with a mean diameter of 2–3 μm. Maintaining a gas bubble at a constant size is technically challenging. Bubbles suspended in a liquid can coalesce, grow or shrink in response to changes in the environment [1]. The surface tension between the gas–liquid interface, the hydrostatic pressure or the acoustic pressure induces consequent diffusion of gas from the gas core into the surrounding liquid. In this way, free gas microbubbles dissolve within seconds after having been introduced in the blood circulation. Smaller bubbles are more susceptible to these influences, because the excess pressure within the bubble that is generated to balance the surface tension inversely scales with the bubble radius, $p_\sigma = 2\sigma/R_0$. This excess pressure tends to raise the partial pressure of the gas inside the bubble to greater than the partial pressure of the gas that is dissolved in the surrounding liquid. Using the equation by Epstein and Plesset [2] dissolution times of gas microbubbles can be calculated.

The Ostwald coefficient (L) is an important parameter for the dissolution of bubbles and is defined as the dimensionless ratio of the solubility of the gas in the liquid to the gas density [3]. Gases with lower Ostwald coefficients dissolve more slowly compared to gases with higher Ostwald coefficients. It is therefore that the newest generation of contrast agents are composed of high molecular weight gases, such as perfluorocarbons (Definity, Sonazoid, and Optison) or sulfur hexafluoride (SonoVue). The diffusion of a gas is inversely proportional to the square root of its molecular weight, the higher the molecular weight, the slower the solubility or diffusion of the gas. Table 1 summarizes the Ostwald coefficients of the different gases used in UCAs and shows the predicted lifetime of a gas bubble with a size of 3 μm in diameter in water. It is assumed that the water is saturated with the gas. Clearly, gases with lower solubility provide the bubbles longer persistence.

Table 1 Ostwald coefficient and disappearance time for 3 μm diameter bubbles containing different gases

	Ostwald coefficient ($\times 10^6$)	Disappearance time (s)
Air	23,168	0.02
Sulfur hexafluoride (Sf_6)	5,950	0.1
Perfluoropropane (C_3F_8)	583	1.1
Perfluorohexane (C_6H_{14})	24	2

Although high molecular weight gases dissolve more slowly compared to air, these free gas microbubbles still do not persist long enough to be of practical use in the human body. A second effective way to slow down dissolution of the microbubbles is the addition of material at the gas–liquid interface. Surfactants such as phospholipids decrease the main driving force for the dissolution of the bubble, which is, as explained above, the surface tension. Other coating materials such as polymers form more rigid encapsulations and support a strain to counter the effect of the surface tension. Current commercially available agents like Sonovue, Definity (both phospholipids), Optison (human albumin), and Sonazoid (lipids) are all coated. The addition of a coating has a strong influence on the microbubble's response to an acoustic pressure. The coating dampens the vibrations of the microbubble and thereby changes the resonance frequency of the microbubbles. This influence of the coating plays a key role in characterizing the behavior of contrast agent microbubbles.

3 The bubble vibration

Microbubbles in a contrast medium react to an external oscillating pressure field with volume pulsations. Depending on the magnitude of the ultrasound wave, the vibrations will be related either linearly or nonlinearly to the applied acoustic pressure. For low acoustic pressures, the instantaneous radius oscillates linearly in relation to the amplitude of the applied external pressure field. For higher amplitudes of the external field, the pulsation of the bubbles becomes nonlinear. In principle, expansion of the bubble is unlimited unlike the compressibility of the bubble.

3.1 Linear bubble vibration

The bubble is considered spherically symmetric and surrounded by a liquid of infinite extent and with a constant viscosity. The bubble volume is defined by a single variable, the radius, and the motion is assumed to be spherically symmetric. The wavelength of the ultrasound field is

assumed to be much larger than the bubble diameter, and only the motion of the bubble surface is of interest. It is assumed that the vapor pressure remains constant during the compression and expansion phase, and that there is no rectified diffusion during the short period of exposure to ultrasound. The gas inside the bubble is assumed to be ideal, and compressed and expanded according to the gas law. At small excitation levels, the displacement of the bubble wall can be compared to the displacement of a simple one-dimensional mass spring oscillator. The oscillator is defined by its mass, restoring force, damping, and applied force. This leads to the equation of motion of the bubble, which is expressed as:

$$m\ddot{x} + \beta\dot{x} + Sx = F_{\text{driv}} \tag{1}$$

where m is the mass of the bubble–liquid system, β is the mechanical resistance related to the dissipation, S is the stiffness of the system, $F_{\text{driv}}(t)$ is the driving force, and $x(t)$ is the radial displacement of the bubble wall relative to the initial radius R_0, according to $x(t) = R(t) - R_0$. Since the motion of the bubble is approximated by the simple harmonic oscillation, the bubble then has it own resonance frequency f_{R}. For an undamped oscillation it is given by:

$$f_{\text{R}} = \frac{1}{2\pi R}\sqrt{\frac{S}{m}} \tag{2}$$

For gas bubbles in a liquid, the stiffness is that of the enclosed volume of gas that acts like a spring when the bubble is disturbed from its equilibrium radius. The inertia is principally due to the mass of the liquid surrounding the bubble that oscillates with it. Medwin [4] has derived values for the mass, the mechanical resistance, and the stiffness as follows:

$$\begin{aligned} m &= 4\pi R_0^3 \rho \\ \beta &= \delta_{tot}\omega m \\ S &= 12\pi\kappa P_0 R_0 \end{aligned} \tag{3}$$

where ρ is the density of the surrounding medium, δ_{tot} is the total damping, ω is the angular frequency, κ is the heat capacity ratio ($C_{\text{p}}/C_{\text{v}}$), and P_0 is the ambient pressure. Substitution of Eq. 3 into Eq. 2 gives the final expression for the resonance frequency for a bubble motion without losses.

$$f_{\text{R}} = \frac{1}{2\pi R}\sqrt{\frac{3\kappa P}{\rho}} \tag{4}$$

This equation shows that the resonant frequency is inversely proportional to the radius. For a diatomic gas such as oxygen or nitrogen, κ equals 1.4. With the aid of this equation the resonance frequency for various bubbles can be calculated, e.g. for a bubble with a diameter of 4 μm, the resonance frequency in water under normal atmospheric pressure is 1.6 MHz.

The damping β in Eq. 1 is determined by three important parameters responsible for the damping: (1) reradiation damping, (2) damping due to the viscosity of surrounding liquid, and (3) thermal damping. The bubble, which can be considered as a secondary source, reradiates ultrasound energy, which decreases the energy of the system. The viscosity of the surrounding fluid, which moves with the bubble wall, causes another source of energy dissipation. Expansion and compression of the bubble cause an increase of the temperature, which results in a net flow of energy outwards into the surrounding medium. The damping coefficients depend on the bubble size and the frequency of the acoustic field and are in the order of 0.1 for bubbles with a diameter between 1 and 10 μm. Exact expressions for the different damping components can be found in [5].

3.2 Nonlinear bubble vibration

If the bubble vibration becomes larger, Eq. 1 does not hold anymore and more sophisticated models are needed. The bubble model developed by Rayleigh provides the theoretical basis in this section. The bubble is considered spherical, and is surrounded by an incompressible liquid of infinite extent. The liquid is assumed to be Newtonian, so its viscosity is constant. The gas in the bubble is compressed and expanded according to the gas law with the polytropic exponent remaining constant during the vibration. A boundary condition is defined for the pressure at the bubble wall at equilibrium. Solving the equations for the conservation of mass and momentum for the gas and the liquid phase results in the (modified) Rayleigh–Plesset equation, which describes the hydrodynamics of the liquid motion around the bubble. Combining the Rayleigh–Plesset equation and the polytropic gas law with the boundary condition, we obtain the following expression, which describes the motion of an ideal gas bubble and proved to be accurate and robust even in the extreme conditions of sonoluminescence [6].

$$\rho_l\left(R\ddot{R} + \frac{3}{2}\dot{R}^2\right) = \left(p_0 + \frac{2\sigma}{R_0}\right)\left(\frac{R}{R_0}\right)^{-3\kappa}\left(1 - \frac{3\kappa}{c}\dot{R}\right) - \frac{2\sigma}{R} - \frac{4\mu\dot{R}}{R} - p_0 - P_{ac}(t) \tag{5}$$

where R $\dot{R}$ and $\ddot{R}$ represent the radius, velocity and acceleration of the bubble wall, ρ_{l} is the density of the liquid, p_0 is the ambient pressure, σ the surface tension, κ is the polytropic gas exponent, μ the viscosity of the surrounding water, c is the speed of sound, and $P_{\text{ac}}(t)$ the applied

acoustic field. For simplicity only the viscous damping caused by the surrounding liquid has been taken into account.

3.3 Coated bubble vibration

Encapsulation of the bubbles dramatically changes their acoustical behavior. The shell causes an increase in resonance frequency due to its stiffness and an increase in damping due to its viscosity. Encapsulated microbubbles were first modeled by De Jong et al. [7] and De Jong and Hoff [8] incorporating experimentally determined elasticity and friction parameters into the Rayleigh–Plesset model. Church [9] used linear visco-elastic constitutive equations to describe the shell. Since then many models have been defined to investigate the influence of the shell on the bubble's vibration, e.g. [10–13].

Recently, Marmottant et al. [14] proposed a new model for phospholipid-coated bubbles. A variable effective surface tension is characteristic for this model. The effective surface tension at the bubble wall varies along three linear regimes. These regimes are inspired by low frequency observations of phospholipid monolayers using Langmuir–Blodgett balances, etc. [14]. The regimes depend on the bubble area, $A = 4\pi R^2$. The model only needs three parameters to describe the effective surface tension: the buckling area of the bubble A_{buckling} below which the surface buckles, an elastic modulus χ that gives the slope of the elastic regime and a critical break-up tension, $\sigma_{\text{break-up}}$, which predicts for which bubble area the coating ruptures with the result that the effective surface tension saturates at σ_{water}. These three regimes can be expressed as follows:

$$\sigma(R) = \begin{cases} 0 & \text{if } R \le R_{\text{buckling}} \\ \chi\left(\frac{R^2}{R^2_{\text{buckling}}} - 1\right) & \text{if } R_{\text{buckling}} \le R \le R_{\text{break-up}} \\ \sigma_{\text{water}} & \text{if } R \ge R_{\text{ruptured}} \end{cases} \tag{6}$$

Including this effective surface tension $\sigma(R)$ in Eq. 5 for the free bubble and adding an extra viscosity term $4\kappa_s/R^2$ for the coating results in the equation of motion for a phospholipid-coated bubble:

$$\rho_l\left(R\ddot{R} + \frac{3}{2}\dot{R}^2\right) = \left(p_0 + \frac{2\sigma(R_0)}{R_0}\right)\left(\frac{R}{R_0}\right)^{-3\kappa}\left(1 - \frac{3\kappa}{c}\dot{R}\right) - \frac{2\sigma(R)}{R} - \frac{4\mu\dot{R}}{R} - \frac{4\kappa_s\dot{R}}{R^2} - p_0 - p_{ac}(t) \tag{7}$$

For small vibration amplitudes within the tensed elastic state, the surface tension can be linearized around a constant value, with $\sigma(R) \approx \sigma(R_0) + 2\chi(R/R_0 - 1)$. Implemented in Eq. 7 it yields the same pressure term $-2\sigma(R)/R = 2\sigma(R_0)/R - 4\chi(1/R_0 - 1/R)$ as in the model proposed by De Jong et al. [15] for thin elastic shells. The shell stiffness coefficient S_p they introduced is related to the present coating elasticity by $S_p = 2\chi$, while their shell friction coefficient is equal to $S_f = 12\pi\kappa_s$. We stress here again that the model by De Jong et al. [15] is limited to small amplitudes of vibration for bounded effective tensions between 0 and $\sigma_{\text{break-up}}$, or for R in between R_{buckling} and R_{ruptured}, while the present model extends the oscillation to unbounded, large amplitudes.

At small acoustic amplitudes the model presented provides a linear radius response to the pressure similar to other Rayleigh–Plesset models with constant surface tension. Under large pressure amplitudes the bubble will experience an original nonlinear response. It will likely buckle in its compression phase which cancels out any surface tension. On the other hand, the surface tension rapidly rises during the expansion phase, and this asymmetry in surface tension provides an asymmetry in capillary pressure, especially strong for small bubbles.

3.4 Simulations

Now we are going to analyze the vibrations of a free gas bubble and a coated bubble using the model by Marmottant et al. [14]. We calculate the responses of the phospholipid-coated contrast agent Sonovue with and without the coating. The coating elasticity and viscosity are measured with a fast framing camera capable of recording the bubble vibration with a frame rate of 25 million frames per second (Van der Meer et al. [16]). By measuring the amplitude of the bubble excursion around resonance (in practice between 0.5 and 6 MHz) and a fit to theoretical prediction, the elasticity and viscosity can be estimated. This results for Sonovue in $\chi = 0.55$ N/m and $\kappa_s = 2.3 \times 10^{-8}$ kg/s. The model by Marmottant et al. [14] requires a third parameter, namely R_{buckling}, which is the radius at which the bubble starts to buckle. Currently, the value of R_{buckling} has yet to be established. We therefore consider two situations: (a) the bubble vibrates solely in its elastic regime and (b) upon compression the bubble will buckle, $R_{\text{buckling}}/R_0 = 1$. We calculate the responses of the bubbles to a driving force consisting of a three cycle waveform with a peak negative amplitude of 50 kPa and a center frequency of 2 MHz. Such an excitation is typical for a clinically used pulse echo-system driven in the fundamental or harmonic mode. The radius of the simulated bubbles is 2.5 μm. The scattered pressure is calculated 1 cm away from the bubble wall.

This yields resonant frequencies of 1.3 MHz for the free gas bubble, 2.2 MHz for the purely elastic coated bubble, and 1.2 MHz for the bubble with a buckling coating. Thus, the bubbles are driven a little below and above their resonant frequency. Figure 1 shows the predicted radial

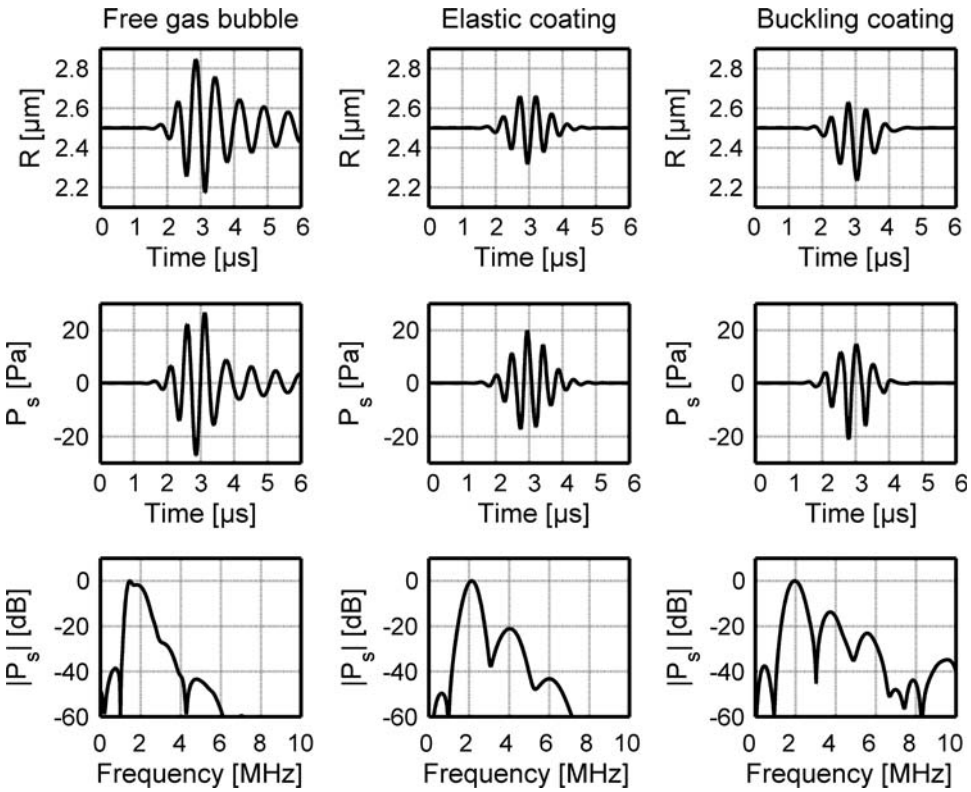

Fig. 1 Vibration of a 2.5-μm free bubble and coated bubble ($\chi = 0.55$ N/m and $\kappa_s = 2.3\ 10^{-8}$ kg/s.) at 2 MHz in water. *Top* radial oscillation, *Middle* scattered pressure at 1 cm, *Bottom* frequency response of scattered pressure

motion of the bubbles (R) and the resulting radiated sound pressures (P_s) as a function of time as well as frequency. The free gas bubble oscillated with the largest amplitude, $\Delta D = 0.7$ μm. The addition of a coating resulted in damping of the oscillation amplitude by a factor of two. The free gas bubble did not immediately stop oscillating after the sound pulse had passed in contrast to the more damped coated bubbles. The effect of coating buckling appears when the results of the elastic coated and buckling coated bubbles are compared. Whereas the elastic coated bubble shows similar expansion and compression phases, the buckling coated bubble expresses a preference for compression. The compression amplitude (0.27 μm) is a factor of two higher than the expansion amplitude (0.13 μm). This asymmetric radial motion leads to elevated harmonic scattering as is shown in the power spectra of the radiated sound pressures.

4 Acoustic characterization

4.1 Linear behavior

Most models include the coating by defining parameters for the coating elasticity and viscosity [8, 9, 11, 14]. The values of these coating parameters are generally unknown. Acoustic measurements can be performed to determine their values. Upon insonification the bubbles absorb as well as scatter energy. In different kinds of acoustic measurements we can determine both the absorbed and the scattered energy by the bubbles.

The energy absorption by a diluted contrast agent is measured in a relatively simple but instructive measurement [7, 8]. We determine the attenuation of the transmitted ultrasound wave by a screen of bubbles as a function of the transmitted frequency. A typical result is given in the left panel of Fig. 2. We diluted 50 μl of the experimental contrast agent BR14 (Bracco Research SA, Geneva, Switzerland) in 175 ml gas saturated water and measured the attenuation using four transducers covering the range from 0.5 to 12 MHz [17]. The results acquired for the different transducers overlap, which shows that this type of measurement is insensitive for the transducer characteristics. The attenuation curve shows a maximum at 1.6 MHz indicating a maximum attenuation for this transmit frequency. At lower frequencies a Rayleigh response appears while for higher frequencies the attenuation decreases and eventually reaches a constant value. The unknown parameters in the theoretical model can now be calculated by a fitting procedure between the measurement and simulation using the size distribution as measured with, e.g. a Coulter Counter. For this fitting procedure in most cases linearized expressions for the absorption and scattering cross sections are applied, which requires the assumption that at the acoustic pressures applied the bubbles behave linearly.

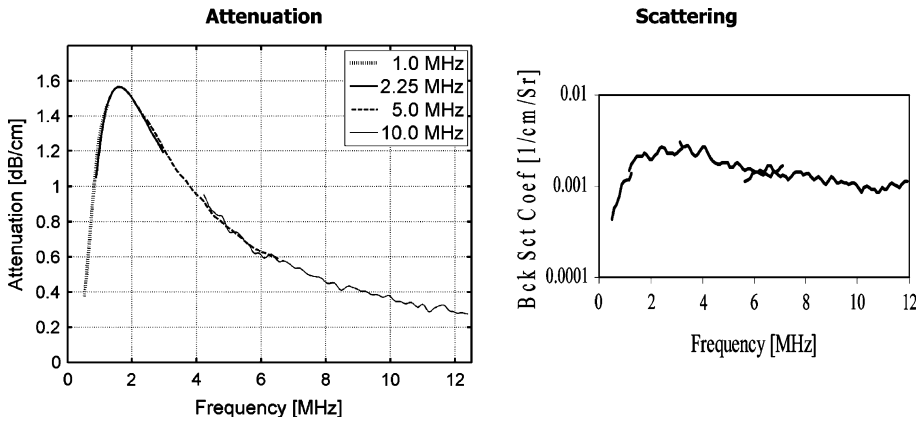

Fig. 2 Attenuation (*left*) and scatter measurements (*right*) as function of the frequency

The scattered energy by the bubbles can be measured using the same transducers in a similar set-up [8]. In contrast to the attenuation, the measured amount of scattered energy depends on the transducer characteristics. The received backscatter signal should therefore be corrected for the transducer frequency response and diffraction of the transmitted ultrasound beam. The resulting backscatter coefficient for diluted Sonovue is presented in the right panel of Fig. 2. The curve shows a steep increase from 1 to 2 MHz and a maximum around 3 MHz. This maximum indicates the resonant frequency of this population of coated bubbles. For higher frequencies the frequency dependency is almost absent as predicted by theory. The scattering of a bubble that is insonified well above resonance is dominated by its own physical cross section. The broad size distribution in the investigated bubble population and relatively high damping of the bubble vibration explain the relatively low and broad peak at 3 MHz.

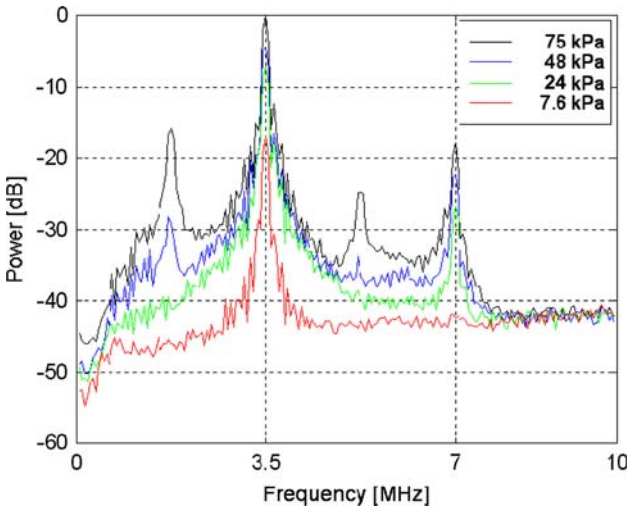

Fig. 3 Harmonic response of Sonovue for four different acoustic pressures (8, 24, 48, 75 kPa). Excitation 3.5 MHz, 10 cycles

4.2 Harmonics

Coated bubbles have been observed to scatter energy at harmonic frequencies at acoustic pressures down to 20–50 kPa. The origin for these harmonics is the nonlinear behavior of the coated bubbles. Nonlinear behavior results in second and higher order harmonics, but also subharmonics and ultraharmonics in the backscattered signal.

To measure the frequency content of the backscattered energy a typical set-up consists of two transducers that are mounted perpendicular with respect to each other. One transducer transmits ultrasound waves and the other receives the backscattered signals generated by the bubbles. Figure 3 shows the results for such an experiment. A narrow banded transducer transmitted sine-wave bursts of 10 cycles at a center frequency of 3.5 MHz. The acoustic pressure was increased from 8 to 75 kPa. The receiver was broad banded and covered the frequency range between 1.5 and 7.5 MHz. We measured the scattering of Sonovue, which was highly diluted to avoid the influence of attenuation by the bubbles [15].

At the lowest acoustic pressure applied (8 kPa), the bubbles only radiated at the transmitted fundamental frequency of 3.5 MHz. When the acoustic pressure was increased to 24 kPa, the bubbles also started to radiate second harmonic energy at 7 MHz. At an acoustic pressure of 48 kPa, we observe in addition to the scattered fundamental and second harmonic frequencies also scattering at the subharmonic frequency. The subharmonic peak at 1.75 MHz is about 25 dB below the fundamental. At the highest acoustic pressure applied of 75 kPa, the bubble scattered even more subharmonic energy than second harmonic energy. Moreover, ultraharmonics appear at this acoustic pressure. Note that 75 kPa, which is equivalent to a mechanical index (MI) of only 0.04, Sonovue bubbles are not destroyed. In the late 1990s, it was believed that subharmonic scattering indicated that the contrast agent was destroyed [18]. At these low acoustic pressures, the uniform elastic shell was supposed to prevent the generation

of subharmonic energy. Currently gained knowledge on the behavior of lipid coatings has changed this view. The Marmottant model is able to predict subharmonic scattering at these low acoustic pressures and we believe that this is the result of the buckling stage of bubble vibration [19].

4.3 Destruction

Many diagnostic imaging techniques are based on the destruction of contrast agents. Soft shelled agents, like Sonovue, Sonazoid, and Optison, resist acoustic pressures up to 100–150 kPa. At higher acoustic pressures, insonification of the bubble leads to changes in its characteristics, but the bubble still may behave as a bubble. For even higher acoustic pressures, e.g. above 300 kPa, the bubbles are destroyed and dissolve completely after a few insonifications.

Hard-shelled polymer contrast agents like PB127 (Point Biomedical Corp, San Carlos, Calif) and Quantison (Quantison; Andaris Ltd., Nottingham, England) do not scatter much at acoustic pressures below 300–500 kPa [20, 21]. At higher acoustic pressures they are destroyed and release their gas content with the result that the backscattered signal increases abruptly for a short time [20, 22]. Moreover, this backscattered signal is highly nonlinear and well suited for harmonic imaging. This effect is transient and lasts until the released free gas bubbles are dissolved in the surrounding liquid.

The destruction of Quantison is investigated in the following measurement [21]. A 1 MHz single element transducer (focus at 75 mm) is mounted in a water tank that contains Quantison (5 ml in 200 ml Isoton). The transducer transmits sine wave bursts of 10 periods with a center frequency of 1 MHz. The repetition rate is 1 Hz. Backscattered ultrasound by the contrast bubbles is received by a 10 MHz broadband transducer. This transducer is mounted perpendicular to the acoustic beam of the transmitting transducer. Figure 4 shows the results of measurements at 300 and 600 kPa of two fresh populations of Quantison at the same concentration. The power spectra of the backscattered energy by the bubbles are calculated by averaging the FFT of ten received traces. The results show mainly fundamental scattering at 300 kPa. When the acoustic pressure amplitude is doubled, we measure a 20-dB increase at the fundamental frequency. More striking is the increase in harmonic scattering. Up to the tenth harmonic frequency (10 MHz) is observed at 600 kPa. A reference measurement using the linear scatterer carborundum, not shown here, reveals that there are no artifacts.

4.4 Single bubble

We have described experiments to characterize UCAs acoustically. In these experiments the contrast agent

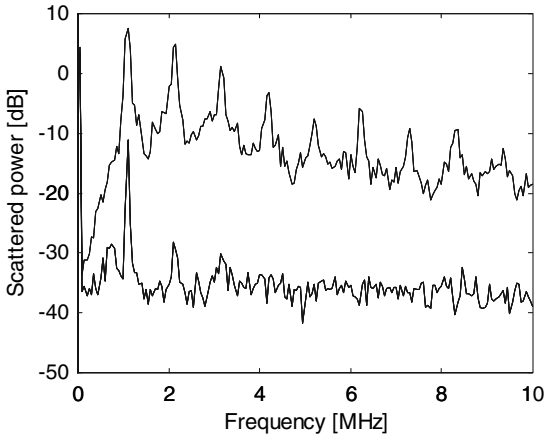

Fig. 4 Received scattered power of Quantison by a 10 MHz transducer. The signal was generated by a 1 MHz transducer transmitting an acoustic pressure of 0.3 MPa (*dashed*) and 0.6 MPa (*solid*)

bubbles were part of a population of bubbles with a certain size distribution. In this way, the results are a weighted summation of all the individual bubbles. Such kinds of methods have of course clinical relevance, but are of limited value for characterizing individual bubbles including their mutual variation. Only in a limited number of studies the scattering of single bubbles has been measured, see, e.g. Shi et al. [23]. One key aspect of the experimental setup is the capability to isolate single bubbles. Single bubbles may be isolated using highly diluted bubble suspensions.

In the experiment that we performed (see [24]), we diluted a suspension of the phospholipid-coated experimental contrast agent BR14 (Bracco Research, Geneva, Switzerland) by a ratio of 1:10,000, which corresponds to 25,000 bubbles per ml. This high dilution rate results in an average of one single bubble in the effective insonified volume of 0.04 µl within the capillary tube (diameter: 200 µm). This corresponds to a statistically averaged distance of 1.5 mm between two adjacent bubbles. In addition, the capillary tube was optically scanned to ensure that there was only one bubble in the acoustic focal area. To ensure that all the bubbles present in the capillary tube were optically observable, smaller bubbles were excluded from the suspension by decantation. As a result 80% of the bubbles in the suspension had a radius larger than 2 µm, which was verified using a Multisizer 3 counter (Beckman-Coulter, Miami, FL).

The left panel of Fig. 5 shows typical examples of single bubble responses measured at an acoustic pressure of 100 kPa. The time traces for bubbles with sizes of $R_0 = 4.6$, 2.1, and 1.5 µm and the corresponding power spectra are displayed. The receiver was calibrated and therefore the results are absolute pressures (Pa). It is observed that the acoustic response of the smallest bubble

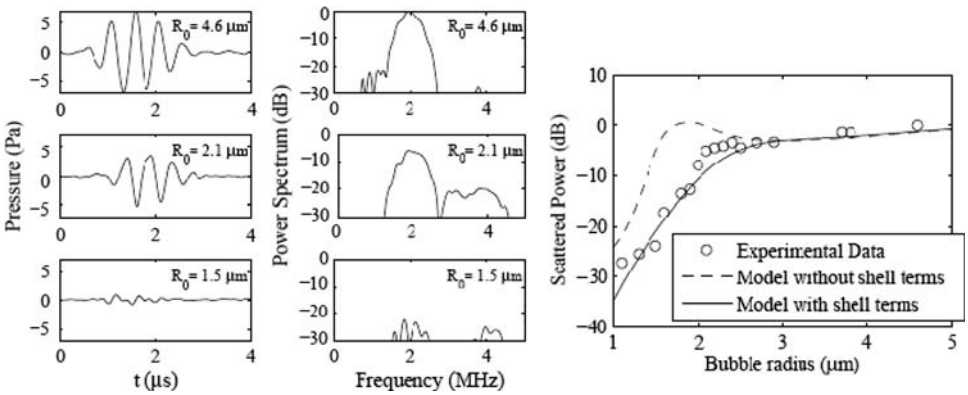

Fig. 5 Measured responses of three single bubbles of three different sizes (4.6, 2.1 and 1.5 μm) excited with a driving pressure of 100 kPa. *Left panel* Measured pressure in Pa. *Right Panel* frequency response (reproduced with permission of JASA 2008)

is 25 dB lower than the maximum response, measured for the largest bubble. This bubble with a resting radius of 1.5 μm is excited below its resonant frequency and hence behaves as a Rayleigh scatterer. The bubble with a radius of $R_0 = 2.1$ μm (middle panel) is excited close to its resonant frequency. The presence of a substantial second harmonic component in its frequency response confirms this observation.

The right panel of Fig. 5 shows more measured scattered powers for bubbles with radii between 1 and 5 μm. We compare the experimentally obtained results (circles) with simulated bubble responses for free gas bubbles (dashed curve) and phospholipid-coated bubbles using the Marmottant model (solid curve). The experimentally obtained results nicely fit the simulated results using the Marmottant model, which shows the influence of the phospholipid coating when the bubbles are insonified below resonance. Above resonance the coated bubbles act like free gas bubbles [24].

5 Optical characterization

In the past research has primarily focused on the sound that bubbles produce. At least as much interesting is the origin of these sounds: the bubble vibration. Looking at bubbles has several advantages over listening. The wavelength of light is much shorter than the wavelength of ultrasound, typically 0.5 and 500 μm, respectively. As a consequence optical observations are more accurate. Furthermore, although it is possible to measure individual bubbles acoustically, measuring bubbles is easier using optical measurements. Generally, in an acoustic experiment even with a high dilution, there are still hundreds of bubbles per wavelength of ultrasound. However, in an optical measurement the size of the bubbles is larger than the wavelength of light with the result that individual bubbles can easily be discriminated.

Chin et al. [25] describe the set-up of an optical measurement system. In this set-up the contrast bubbles are injected in a capillary tube which is mounted in a water tank. The water tank stands below a microscope that magnifies the bubbles by a factor of 240. A fast framing camera is attached to the microscope. Such a fast framing camera is necessary to record images at an extremely high frame rate. An average video camera does not suffice because it records at most 25 images per second, while the bubbles vibrate at frequencies in the order of MHz. Experience has shown that in order to evaluate periodic phenomena accurately, the sampling rate should exceed the frequency of the phenomenon by at least a factor 8–10. The fast framing camera used in this set-up was purpose-built and is able to record at a frame rate of 25 million frames per second. The core of the camera system is a fast rotating mirror (max. 20,000 rps), which sweeps images of the bubbles along 128 charge coupled devices (CCDs). The camera system records in one experiment six movies of 128 frames with an interval time of 80 ms between the movies. The camera system was called "Brandaris 128" after a famous lighthouse in the Netherlands [25].

5.1 Small and medium acoustic pressure

Figure 6 presents an example of a recording with the Brandaris fast framing camera. The figure shows an isolated bubble with a size of 4.2 μm in diameter that was insonified with an acoustic pressure of 250 kPa at a frequency of 1.7 MHz. In 64 frames the bubble was observed before, during and after the ultrasound pulse. In the first 13 frames, the microbubble is at rest. Starting at frame 14, the microbubble is first compressed, and then reaches within six cycles a maximum diameter of 5.4 μm and a minimum diameter of 2.6 μm. In each image frame the bubble diameter was established. The resulting diameter–time (D–T) curve is shown in the panel in the middle and the corresponding power spectrum in the right panel. This experimentally obtained D–T curve can be compared directly with a simulated D–T curve, which is a great advantage compared to acoustic experiments. In an acoustic experiment scattered sound pressures are

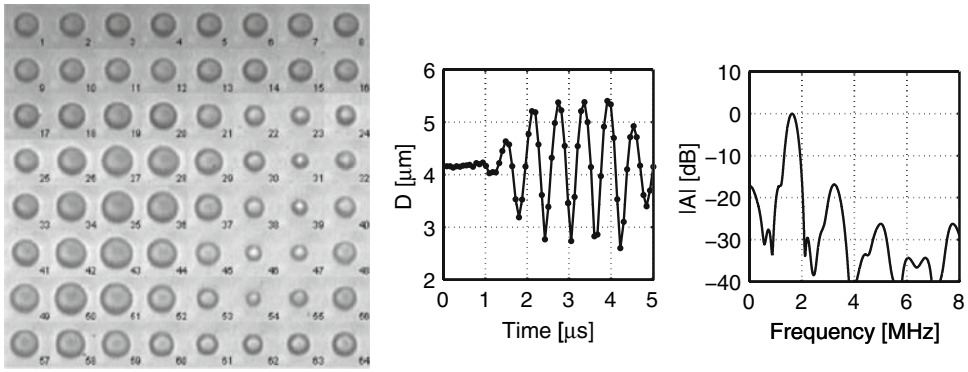

Fig. 6 **a** Sequence of 64 image frames of a 4.2 μm diameter microbubble, driven by a 6-cycle—US burst with a peak negative pressure of 250 kPa. **b** Diameter–time response. **c** Power spectrum of diameter–time response

measured instead of radial responses. Therefore, before simulated and acoustic results can be compared, scattered sound pressures must be calculated from the simulated radial responses. This can be done using [26]

$$P_s = \rho_l \frac{R}{r}\left(2\dot{R}^2 + R\ddot{R}\right). \quad (8)$$

Using the fast framing camera several interesting studies on individual bubbles have been performed. An example is the determination of the bubble's resonant frequency. This has been achieved by repeatedly insonifying the bubbles, whereby the transmit frequency is varied over the different recordings. Because the Brandaris is able to record six movies of 128 frames, or 12 movies of 64 frames, etc., such an experiment can be done within one run in 2 s. From the recorded images a resonance curve can be constructed showing the resonance peak and width. This method, termed microbubble spectroscopy has recently been described by Van der Meer et al. [16].

Figure 7 shows another example of the strength of optical measurements. The left panel displays an image frame containing several bubbles that are quite close together (<20 μm). The bubbles have been insonified with an ultrasound pulse of 1 MHz and 200 kPa. The ultrasound field has a wavelength of 1.5 mm, which is much larger than the size of the bubbles. The bubbles therefore all experience the same ultrasound field. This, however, did not result in identical responses for all bubbles. This is most clear when we compare the bubble with a size of 6 μm in diameter (No 2) with the bubble with the largest size of 10 μm in diameter (No 4). At $t = 5$ μs, we observe a 180° phase difference between both bubble responses. Such behavior is typical for harmonic oscillators. When the oscillator is insonified below resonance, it responds in phase with the driving force. Above resonance, inertia dominates and the response will be out of phase with the driving force. A bubble that is insonified at its resonant frequency will respond with a 90° phase difference compared to the phase of the driving force. Based on our observations we conclude that the resonant size for a transmit frequency of 1 MHz must be between 6 and 10 μm in diameter.

5.2 Destruction

Optical recordings are important resources when the destruction of contrast bubbles is investigated. The

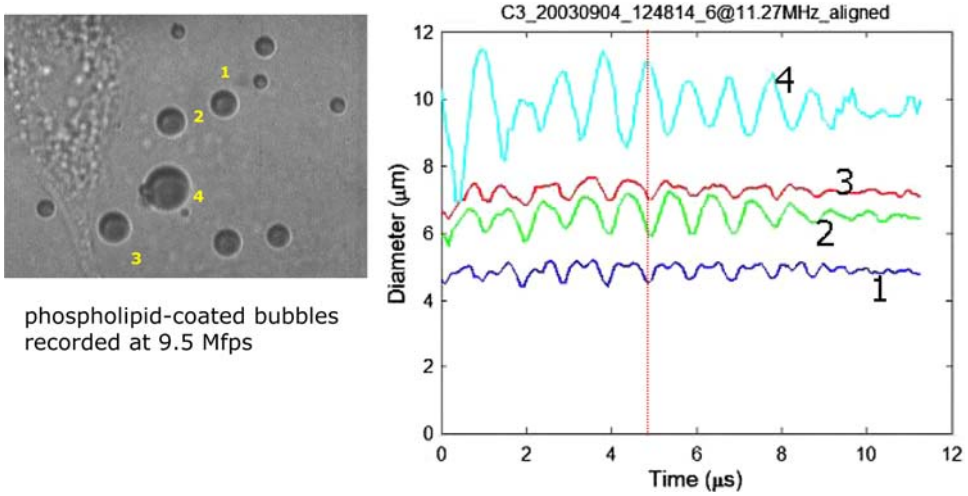

Fig. 7 Bubbles images at 1 MHz and 200 kPa with the Brandaris fast framing camera. *Right panel* the corresponding D–T curves

recordings may help to reveal which factors amplify or reduce the destruction process. This is relevant for UCA destruction replenishment methods [27], which are frequently used in the clinic to quantify tissue perfusion. In this method, an initial high intensity ultrasound pulse destroys all the bubbles present in the tissue and subsequently lower intensity pulses are applied to measure the rate of inflow of fresh bubbles in the tissue. Furthermore, bubble destruction can be used to detect bubbles for contrast-enhanced imaging. The released bubbles generate highly nonlinear sound pressures with a high intensity, which is well suited for harmonic imaging (see also Sect. 4) [22]. A totally different application of bubble destruction is found in drug delivery applications [28, 29] and in future bubble destruction may be part of blood pressure measurements [30].

The destruction mechanism of a contrast agent depends mainly on the coating of the bubbles as explained above. For rigid shelled contrast agents such as Quantison and PB127, the destruction of the microbubbles is accompanied by shell rupture and gas release and the formation of new free gas bubbles [20, 31]. In Fig. 8, we show the formation of new free gas bubbles from the "mother" PB127 microbubble. In this experiment, two different ultrasound bursts were transmitted sequentially. The first ultrasound burst, which consisted of four cycles of a sine wave, an MI of 1.4 and a frequency of 1.7 MHz, cracked the shell of the bubble. The released free gas bubbles were interrogated within the same optical recording, 1 μs later, by applying a second similar ultrasound burst with an MI of 0.25. The frame rate of the optical recordings was 11.5 MHz. The first six frames of the upper row of Fig. 8 show shell destruction and gas escaping from the microbubble due to the high MI burst. In the next six frames (from 41 to 60), we observe the creation of two new free gas bubbles next to the original microbubble. As a result of the second (non-destructive) ultrasound burst these newly formed free gas bubbles started to vibrate.

6 Bubble ambiguities and other phenomena

Some years of experience with the Brandaris fast framing camera produced a lot of interesting observations of bubble behavior. Many of these observations do not fit in the "classical" representation of the bubble as a nonlinear oscillator. Here we provide for a short overview.

6.1 Mode vibration of bubbles

To study bubble dynamics (modified) Rayleigh–Plesset models like Eqs. 5 and 7 are frequently used. These models are based on the assumption that the bubbles oscillate spherically. In practice, however, oscillating bubbles may show various intriguing shapes, see, e.g. [32, 33]. Non-spherical bubble shapes as displayed in Fig. 9 can be categorized by decomposition of the shape into spherical harmonics. In a study on 20–100 micron sized free gas bubbles, it was observed that bubbles can obtain stable surface modes when irradiated at their resonance frequency

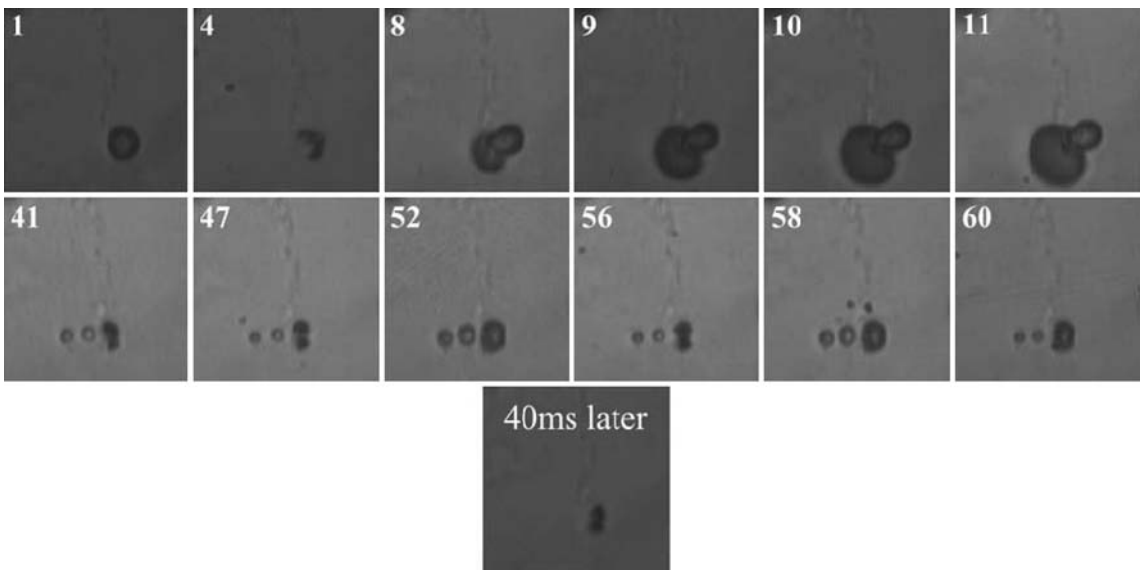

Fig. 8 Optical frames showing initial PB127 microbubble (frame 1), shell fissure and gas escape (frames *4*, *8–11*) under ultrasound of 1.7 MHz, four cycles, MI 1.4 and formation of new free bubbles. Two new free bubbles (frames *41*, *47–60*) demonstrating oscillations under ultrasound of 1.7 MHz, four cycles and MI 0.25. Last displayed frame shows an optical recording performed 40 ms later, demonstrating bubble disappearance due to dissolution

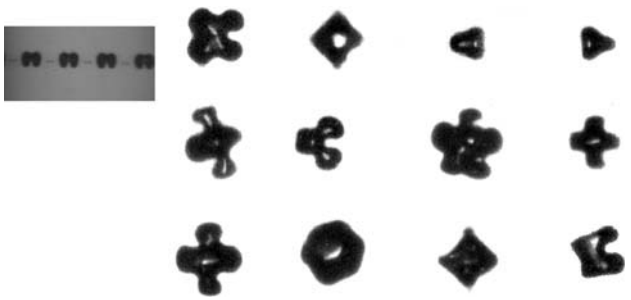

Fig. 9 Vibration modes

[33]. At resonance, optical recordings showed spherical harmonic orders up to 4 (rectangular, see Fig. 9). Bubbles undergoing surface modes have been reported to generate subharmonic frequencies. Optical studies supported this observation by showing that the frequency of the surface mode corresponded to half the transmit frequency [33].

6.2 Compression only

The responses of Sonovue contrast bubbles were investigated in a large study. The bubbles were insonified using three different acoustic pressures and three different transmit frequencies. It appeared that 40% of the observed bubbles showed so-called compression-only behavior [34]. Microbubbles showing this behavior compress, but hardly expand. This is opposite to "normal" nonlinear bubble oscillation, whereby in principle expansion is infinite in contrast to compression of the gas core. Compression-only behavior is typically induced by the presence of the phospholipid coating [14]. Coated bubbles displaying compression-only behavior are expected to be highly beneficial for nonlinear acoustic imaging. Bubbles oscillating in this mode are in fact tailor-made for pulse-inversion imaging [35].

6.3 Onset of the bubble vibration

"Classical" theory on coated bubbles predicts a linear onset to vibration, which means that any acoustic pressure applied to the bubble leads to its vibration. Recordings with the Brandaris fast framing camera revealed that specific phospholipid-coated bubbles do not start to vibrate according to this linear onset, but these microbubbles show what has been termed "threshold behavior" [36]. Bubbles showing this behavior need an initial acoustic pressure before any vibration is observed. Coated bubbles were supposed to attenuate proportional to the acoustic pressure applied. The recent observations of pressure-dependent attenuation [37] may well be explained by the occurrence of threshold behavior [17]. An imaging technique such as power modulation imaging profits from threshold behavior as has been described by Emmer et al. [38]. It should be mentioned that compression-only behavior as well as threshold behavior is predicted by the Marmottant model [14].

6.4 Vibration of bubbles in contact with a wall

Optical studies on bubble vibration are usually performed in a two-dimensional (2D) image plane. The bubble is positioned in an acoustically and optically transparent capillary tube, where it floats to the top side of the tube and stays at this position against the tube wall. This has practical advantages, because it allows precise optical as well as acoustical focusing. It has, however, the disadvantage that the wall might influence the radial motion of the bubble.

The influence of the wall on the bubble vibration was studied using a set-up including a microscope with two objectives. One objective imaged the bubble from the top and one objective was positioned orthogonally such that we obtained a quasi-instantaneous 3D image sequence of a coated bubble touching a rigid wall [39]. The bubble showed a tendency to vibrate axial-symmetrically around the axis normal to the wall, but asymmetrically in the direction perpendicular to the wall. In the past, the asymmetric oscillation was thought to be much smaller than the radial oscillation for coated bubbles. However, it appeared that the vibration is strongly asymmetrical at frequencies and pressures relevant for the clinic (140 kPa at 1 MHz, mechanical index of 0.14).

6.5 Bubble vibration at varying distance to the wall

A cloud of bubbles responds differently when attached to the wall compared to freely floating bubbles. An optical tweezer (laser trap) was used to measure the response of single bubbles at varying distances from a rigid wall [40]. The optical tweezer controlled the position of the single bubble, while the vibration of the bubble was recorded with the Brandaris camera. It was verified that the laser trap did not influence the bubble dynamics, but still the microbubble was temporarily released from the laser trap during the experiment. The study revealed that the amplitude of the bubble oscillation decreased with decreasing distance to the wall at a fixed frequency.

7 Conclusion

UCAs consist of encapsulated bubbles with sizes between 1 and 10 μm diameter. The encapsulation stabilizes the microbubble, which is required in a clinical setting. It takes about 15–60 s after intra venous injection before the agent

reaches the myocardium, liver, kidney and other organs. Unencapsulated bubbles of the same size would disappear within a few milliseconds. The encapsulation also changes the acoustic behavior of the bubble. The most dominant influences of the encapsulation are the increased elasticity which changes the resonance frequency and the viscosity which increases the damping of the vibration. Basically there are two ways to characterize a contrast agent: acoustically by measuring the attenuation and scattering and optically where the vibrations of individual bubbles are recorded with a fast framing camera. The advantage of acoustical characterization is that it measures the average response of all bubbles in the agent. Assuming that the size distribution can be measured by other means (e.g., coulter counter) it is possible to calculate the average elasticity and viscosity of the encapsulation from these measurements. The advantage of optical measurements is that the elasticity and viscosity can be deduced for individual bubbles. In this way the dependency of the elasticity and viscosity on the diameter can be easily recorded and even the variation of these parameters for bubbles of the same size. A clear disadvantage of optical characterization is that one has to do a lot of measurements to characterize the whole size distribution, while for acoustic measurements, an average value can be deduced from only one measurement.

References

1. van Liew HD, Burkard ME (1995) Behavior of bubbles of slowly permeating gas used for ultrasonic imaging contrast. Invest Radiol 30:315–321. doi:10.1097/00004424-199505000-00008
2. Epstein PS, Plesset MS (1950) On the stability of gas bubbles in liquid-gas solutions. J Chem Phys 18:1505–1509. doi:10.1063/1.1747520
3. Kabalnov A, Klein D, Pelura T, Schutt E, Weers J (1998) Dissolution of multicomponent microbubbles in the bloodstream: 1. Theory. Ultrasound Med Biol 24:739–749. doi:10.1016/S0301-5629(98)00034-9
4. Medwin H (1977) Counting bubbles acoustically: A review. Ultrasonics 15:7–13. doi:10.1016/0041-624X(77)90005-1
5. de Jong N, Bouakaz A, Frinking P (2002) Basic acoustic properties of microbubbles. Echocardiography 19:229–240. doi:10.1046/j.1540-8175.2002.00229.x
6. Brenner MP, Hilgenfeldt S, Lohse D (2002) Single-bubble sonoluminescence. Rev Mod Phys 74:425–484. doi:10.1103/RevModPhys.74.425
7. de Jong N, Hoff L, Skotland T, Bom N (1992) Absorption and scatter of encapsulated gas filled microspheres: theoretical considerations and some measurements. Ultrasonics 30:95–103. doi:10.1016/0041-624X(92)90041-J
8. de Jong N, Hoff L (1993) Ultrasound scattering properties of Albunex microspheres. Ultrasonics 31:175–181. doi:10.1016/0041-624X(93)90004-J
9. Church CC (1995) The effect of an elastic solid surface layer on the radial pulsations of gas bubbles. J Acoust Soc Am 97:1510–1521. doi:10.1121/1.412091
10. Allen JS, Rashid MM (2004) Dynamics of a hyperelastic gas-filled spherical shell in a viscous fluid. J Appl Mech 71:195–200. doi:10.1115/1.1653722
11. Hoff L, Sontum P, Hovem J (2000) Oscillations of polymeric microbubbles: effect of the encapsulating shell. J Acoust Soc Am 107:2272–2280. doi:10.1121/1.428557
12. Morgan KE, Allen JS, Dayton PA, Chomas JE, Klibanov AL, Ferrara KW (2000) Experimental and theoretical evaluation of microbubble behavior: effect of transmitted phase and bubble size. IEEE Trans Ultrason Ferroelectr Freq Control 47:1494–1509. doi:10.1109/58.883539
13. Sarkar K, Shi WT, Chatterjee D, Forsberg F (2005) Characterization of ultrasound contrast microbubbles using in vitro experiments and viscous and viscoelastic interface models for encapsulation. J Acoust Soc Am 118:539–550. doi:10.1121/1.1923367
14. Marmottant P, van der Meer S, Emmer M, Versluis M, de Jong N, Hilgenfeldt S, Lohse D (2005) A model for large amplitude oscillations of coated bubbles accounting for buckling and rupture. J Acoust Soc Am 118:3499–3505. doi:10.1121/1.2109427
15. de Jong N, Cornet R, Lancee CT (1994) Higher harmonics of vibrating gas filled microspheres. Part two: measurements. Ultrasonics 32:455–459. doi:10.1016/0041-624X(94)90065-5
16. van der Meer SM, Dollet B, Voormolen MM, Chin CT, Bouakaz A, de Jong N, Versluis M, Lohse D (2007) Microbubble spectroscopy of ultrasound contrast agents. J Acoust Soc Am 121:648–656. doi:10.1121/1.2390673
17. Emmer M, Vos HJ, Goertz DE, van Wamel A, Versluis M, de Jong N (2009) Pressure-dependent attenuation and scattering of phospholipid-coated microbubbles at low acoustic pressures. Ultrasound Med Biol 35:102–111. doi:10.1016/j.ultrasmedbio.2008.07.005
18. Lotsberg O, Hovem JM, Aksum B (1996) Experimental observation of subharmonic oscillations in Infoson bubbles, vol 99. ASA, USA, pp 1366–1369
19. Frinking P, Gaud E, Arditi M (2009) Compression-only behavior and subharmonic scattering of phospholipid-shell microbubbles. In: Abstracts of the 14th European Symposium on Ultrasound Contrast Imaging, pp 80–87
20. Bouakaz A, Versluis M, de Jong N (2005) High-speed optical observations of contrast agent destruction. Ultrasound Med Biol 31:391–399. doi:10.1016/j.ultrasmedbio.2004.12.004
21. Frinking PJA, de Jong N, Céspedes EI (1999) Scattering properties of encapsulated gas bubbles at high ultrasound pressures. J Ac Soc Am 105:1989–1996. doi:10.1121/1.426732
22. Frinking PJA, Céspedes EI, Kirkhorn J, Torp H, de Jong N (2001) A new ultrasound contrast imaging approach based on the combination of multiple imaging pulses and a separate release burst. IEEE Trans Ultrason Ferroelectr Freq Control 48:643–651. doi:10.1109/58.920687
23. Shi WT, Forsberg F, Bautista R, Vecchio C, Bernardi R, Goldberg BB (2004) Image enhancement by acoustic conditioning of ultrasound contrast agents. Ultrasound Med Biol 30:191–198. doi:10.1016/j.ultrasmedbio.2003.10.007
24. Sijl J, Gaud E, Frinking PJA, Arditi M, de Jong N, Lohse D, Versluis M (2008) Acoustic characterization of single ultrasound contrast agent microbubbles. J Acoust Soc Am 124:4091–4097. doi:10.1121/1.2997437
25. Chin CT, Lancee C, Borsboom J, Mastik F, Frijlink M, de Jong N, Versluis M, Lohse D (2003) Brandaris 128: a 25 million frames per second digital camera with 128 highly sensitive frames. Rev Sci Instrum 74:5026–5034. doi:10.1063/1.1626013

26. Hilgenfeldt S, Lohse D, Zomack M (1998) Response of bubbles to diagnostic ultrasound: a unifying theoretical approach. Eur Phys J B4:247–255. doi:10.1007/s100510050375
27. Wei K, Jayaweera AR, Firoozan S, Linka A, Skyba DM, Kaul S (1998) Quantification of myocardial blood flow with ultrasound-induced destruction of microbubbles administered as a constant venous infusion. Circulation 97:473–483
28. Dijkmans PA, Juffermans LJ, Musters RJ, van Wamel A, ten Cate FJ, van Gilst W, Visser CA, de Jong N, Kamp O (2004) Microbubbles and ultrasound: from diagnosis to therapy. Eur J Echocardiogr 5:245–256. doi:10.1016/j.euje.2004.02.001
29. Unger EC, Porter T, Culp W, Labell R, Matsunaga T, Zutshi R (2004) Therapeutic applications of lipid-coated microbubbles. Adv Drug Deliv Rev 56:1291–1314. doi:10.1016/j.addr.2003.12.006
30. Bouakaz A, Frinking PJA, de Jong N, Bom N (1999) Noninvasive measurement of the hydrostatic pressure in a fluid-filled cavity based on the disappearance time of micrometer-sized free gas bubbles. Ultrasound Med Biol 25:1407–1415. doi:10.1016/S0301-5629(99)00109-X
31. Frinking PJA, Bouakaz A, Kirkhorn J, Ten Cate FJ, de Jong N (2000) Ultrasound contrast imaging: current and new potential methods. Ultrasound Med Biol 26:965–975. doi:10.1016/S0301-5629(00)00229-5
32. Dollet B, van der Meer SM, Garbin V, de Jong N, Lohse D, Versluis M (2008) Nonspherical oscillations of ultrasound contrast agent microbubbles. Ultrasound Med Biol 34:1465–1473. doi:10.1016/j.ultrasmedbio.2008.01.020
33. Palanchon P (2004) Ultrasound harmonic classification of microemboli. Ph.D. dissertation, Erasmus University Rotterdam
34. de Jong N, Emmer M, Chin CT, Bouakaz A, Mastik F, Lohse D, Versluis M (2007) "Compression-only" behavior of phospholipid-coated contrast bubbles. Ultrasound Med Biol 33:653–656. doi:10.1016/j.ultrasmedbio.2006.09.016
35. Burns PN, Wilson T, HSD (2000) Pulse inversion imaging of liver blood flow: an improved methode for characterization of focal masses with microbubble contrast. Invest Radiol 35:58–71. doi:10.1097/00004424-200001000-00007
36. Emmer M, van Wamel A, Goertz DE, de Jong N (2007) The onset of microbubble vibration. Ultrasound Med Biol 33:941–949. doi:10.1016/j.ultrasmedbio.2006.11.004
37. Tang M-X, Eckersley RJ, Noble JA (2005) Pressure-dependent attenuation with microbubbles at low mechanical index. Ultrasound Med Biol 31:377–384. doi:10.1016/j.ultrasmedbio.2004.12.009
38. Emmer M, Vos HJ, van Wamel A, Goertz DE, Versluis M, de Jong N (2007) Clinical relevance of pressure-dependent scattering at low acoustic pressures. Ultrasonics 47:74–77. doi:10.1016/j.ultras.2007.07.004
39. Vos HJ, Dollet B, Bosch JG, Versluis M, Jong Nd (2008) Nonspherical vibrations of microbubbles in contact with a wall—a pilot study at low mechanical index. Ultrasound Med Biol 34:685–688
40. Garbin V, Cojoc D, Ferrari E, Di Fabrizio E, Overvelde MLJ, van der Meer SM, de Jong N, Lohse D, Versluis M (2007) Changes in microbubble dynamics near a boundary revealed by combined optical micromanipulation and high-speed imaging. Appl Phys Lett 90:114103. doi:10.1063/1.2713164